ACS APPLIED ELECTRONIC MATERIALS

pubs.acs.org/acsaelm Article

Isothermal Heteroepitaxy of $Ge_{1-x}Sn_x$ Structures for Electronic and Photonic Applications

Omar Concepción,* Nicolaj B. Søgaard, Jin-Hee Bae, Yuji Yamamoto, Andreas T. Tiedemann, Zoran Ikonic, Giovanni Capellini, Qing-Tai Zhao, Detlev Grützmacher, and Dan Buca

Cite This: *ACS Appl. Electron. Mater.* 2023, 5, 2268−2275 Read Online

ACCESS | Metrics & More | Article Recommendations | Supporting Information

ABSTRACT: Epitaxy of semiconductor-based quantum well structures is a challenging task since it requires precise control of the deposition at the submonolayer scale. In the case of $Ge_{1-x}Sn_x$ alloys, the growth is particularly demanding since the lattice strain and the process temperature greatly impact the composition of the epitaxial layers. In this paper, the realization of high-quality pseudomorphic $Ge_{1-x}Sn_x$ layers with Sn content ranging from 6 at. % up to 15 at. % using isothermal processes in an industry-compatible reduced-pressure chemical vapor deposition reactor is presented. The epitaxy of $Ge_{1-x}Sn_x$ layers has been optimized for a standard process offering a high Sn concentration at a large process window. By varying the N_2 carrier gas flow, isothermal heterostructure designs suitable for quantum transport and spintronic devices are obtained.

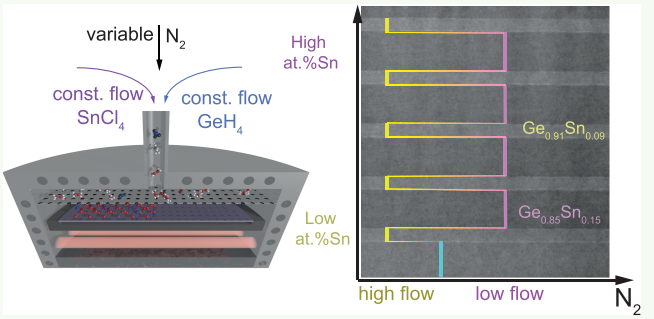

KEYWORDS: *GeSn alloy, chemical vapor deposition, isothermal heterostructures, epitaxial growth, optoelectronic applications*

INTRODUCTION

Group-IV $Ge_{1-x}Sn_x$ alloys are attracting ever-growing interest as enablers of the extension of the Si-photonics technological platform toward the near-/mid-infrared region (NIR/MIR) of the electromagnetic spectrum. This comes following the experimental demonstration of a unique property for the group-IV semiconductors, a fundamental direct band gap in $Ge_{1-x}Sn_x$ alloys[1] that led to the realization of optically pumped lasers up to room temperature[2] and also electrically injected $Ge_{1-x}Sn_x$ lasers operating at low temperatures.[3] Moreover, the previously short-wave infrared range dominated by III-V materials was reached and extended into MIR as demonstrated recently by Ge/$Ge_{1-x}Sn_x$ single pixel imagers on Si.[4]

Furthermore, the $Ge_{1-x}Sn_x$ material system is making its way into a diversity of research fields, such as nanoelectronics,[5] thermoelectrics,[6] spintronics,[7] and quantum computing.[8] Due to their strong spin−orbit coupling (SOC), holes in Ge have emerged as one of the most promising spin qubit candidates.[9,10] To further enhance the SOC strength, materials with higher atomic numbers are preferred due to larger atomic potential variation, which is achieved by the incorporation of Sn atoms into Ge crystals.[11]

Different from laser structures, which typically require thick layers and very large Sn contents, to widely separate the Γ and L- valleys of the conduction band, for electronic transport thin defect-free $Ge_{1-x}Sn_x$ layers or quantum wells (QWs) heterostructures are desirable. Such advanced heterostructures, which employ Ge or $Si_{1-x-y}Ge_ySn_x$ barrier layers to define $Ge_{1-x}Sn_x$ QWs, are extremely challenging for the epitaxial growth.[12] For example, even the simple growth of a stack in which a $Ge_{1-x}Sn_x$ layer is deposited on another $Ge_{1-y}Sn_y$, $x < y$ layer (inverse step Sn composition) cannot be easily performed. Indeed, to get a lower Sn content, one typically has to increase the deposition temperature. However, this temperature increase leads to crystallinity degradation of the already grown layer(s) via Sn diffusion or even segregation.[13] Therefore, the layer with the highest Sn content in a heterostructure defines the maximum growth temperature for the epitaxy of a complex heterostructure.[14−16] Presently, to circumvent the problems of large lattice mismatch, large built-in compressive strain, and low Sn solubility, high Sn content $Ge_{1-x}Sn_x$ layers have been grown on micrometer-thick $Ge_{1-x}Sn_x$ buffers where the Sn content is increased gradually or in small steps.[17] This approach limits the scalability and consequently the applicability of these structures, for example, for metal oxide semiconductor field-effect transistors (MOSFETs).

Two commercially available Ge precursors, germane (GeH_4) and digermane (Ge_2H_6), are commonly used in (Si)GeSn

Received: January 25, 2023
Accepted: March 21, 2023
Published: April 3, 2023

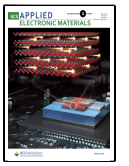

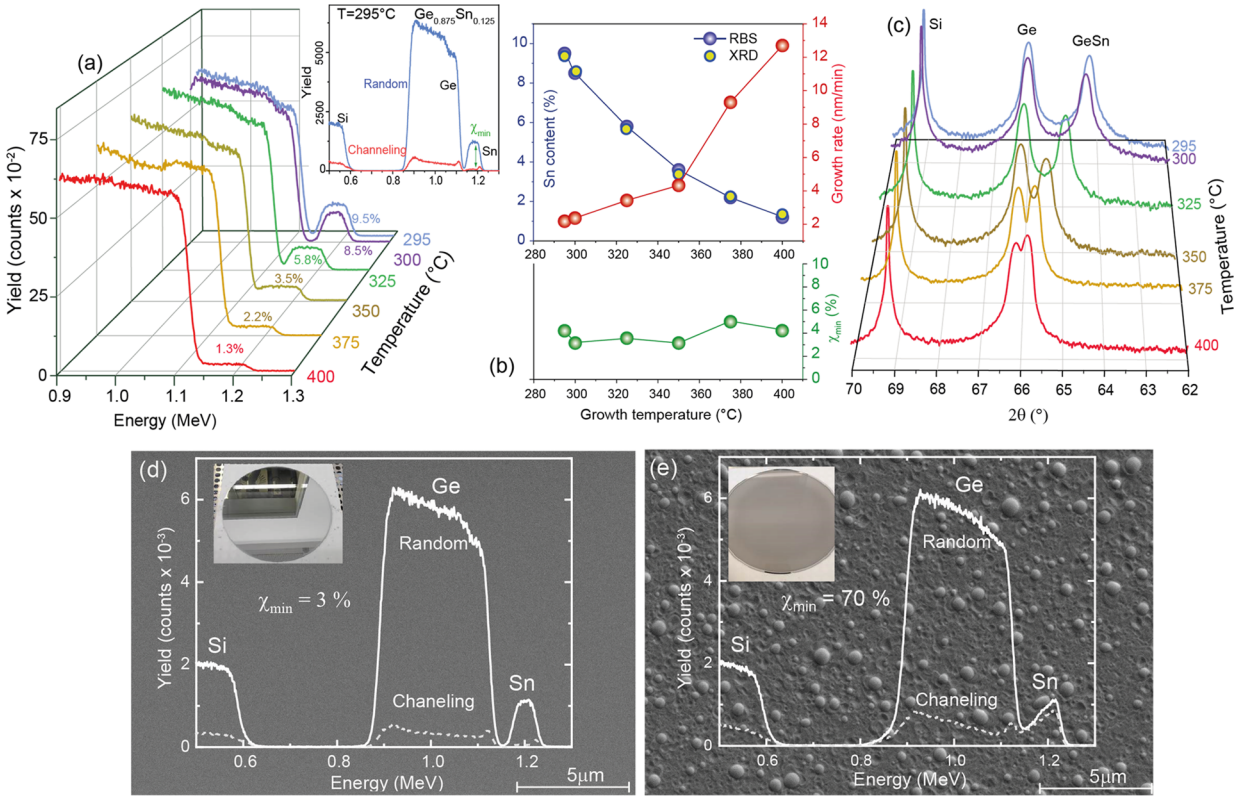

Figure 1. (a) 3D plot of RBS random spectra of $Ge_{1-x}Sn_x$ layers grown at different process temperatures. Inset: the full random and channeling spectra of the sample grown at 295 °C. (b) Sn content, growth rate, and the RBS minimum channeling yield as a function of the substrate temperature. (c) Symmetric 2θ-ω XRD spectra along the (004) plane of the same set of samples. SEM and optical images (inset) of samples with (d) mirror-like and (e) Sn segregation surfaces overlapped with the RBS random and channeling spectra.

chemical vapor deposition (CVD) reactors, while $SnCl_4$ is the precursor of choice for the Sn atoms. The increased reactivity of Ge_2H_6 at low growth temperatures and the resulting high growth rates makes it ideal for the epitaxy of thick relaxed layers.[1,18] However, Ge_2H_6 is significantly more expensive than GeH_4, has limited availability, and the films may be accompanied by the formation of defects.[19−21] On the other hand, GeH_4 offers lower growth rates and a narrower window of the growth parameters, like the reactor pressure, gas flow rates, and temperature, which offers high crystallinity Sn-rich $Ge_{1-x}Sn_x$ alloys.[22,23] It then becomes clear that these parameters have a strong impact on the gas phase reactions of different molecules like GeH_4 and Ge_2H_6. The preferred reaction partner for the stable $SnCl_4$ molecule on the substrate surface are GeH_x (x = 1,2,3) radicals. The formation of those in the gas phase is heavily impacted by the aforementioned growth parameters. An additional parameter suitable to influence gas phase reactions is the composition of the carrier gas, i.e., mixtures of H_2 and N_2.[24] A high H_2 concentration reduces the cracking rate of GeH_4 and Ge_2H_6 when compared to the high N_2 concentration and increases the back-reaction rate from GeH_x-radicals to GeH_4 molecules. However, it has to be kept in mind that the H_2 ambient supports the hydrogen passivation of the surface, preventing Ge segregation[25] as well as surface oxidation.[26] Most importantly, the molecules prepared by gas phase reactions at the substrate surface are crucial for the subsequent surface kinetics guiding the CVD growth at low temperatures.[27]

In this paper, the epitaxy of thin $Ge_{1-x}Sn_x$ alloys using GeH_4 and $SnCl_4$ precursors is revisited, targeting a simple methodology that uses the N_2 gas flow as the main growth parameter to realize isothermal heterostructures. In particular, the growth of layer sequences, like quantum wells with large variations of Sn concentration in the $Ge_{1-x}Sn_x$ heterostructures, is enabled by keeping the process temperature, the reactor pressure, and the flow of the gas precursors constant. In this way, the gas flow rate and the partial pressure of the precursors change, and the gas phase reactions are thus modified with impact on the surface kinetics, allowing precise control of the Sn concentration. The knowledge gained is exploited to realize isothermally epitaxial GeSn-based heterostructures aimed for electronic-, spintronic-, and photonic-device applications.

EXPERIMENTAL METHODS

The $Ge_{1-x}Sn_x$ epitaxy was performed in an industry compatible 300 mm/200 mm AIXTRON TRICENT reduced-pressure chemical vapor deposition (RP-CVD) reactor with a showerhead technology that provides a small reactor volume and a uniform gas precursor distribution over the whole wafer. Si (001) wafers (200 mm) were cleaned *ex situ* with HF vapor using an automated cleaning tool, followed by an *in situ* pre-epi bake at about 1000 °C. Two types of Ge/Si substrates were used to reduce the lattice mismatch between $Ge_{1-x}Sn_x$ and the Si substrate: (i) a 300 nm-thick Ge buffer layer grown at 450 °C on Si (001) substrates before the $Ge_{1-x}Sn_x$ layer deposition (one epitaxy run) and (ii) a previously grown 1.5 μm-thick, high quality, cycle-annealed Ge/Si(001) virtual substrate (VS) (see details in ref 28).

Germane, GeH_4 (10% diluted in H_2), and tin-tetrachloride ($SnCl_4$) precursors were employed, while N_2 was used as carrier gas. Based on previous $Ge_{1-x}Sn_x$ growth experience using Ge_2H_6,[29] in agreement with the literature reports,[30] the precursor flow was scaled and adjusted to obtain mirror-like wafers with high-quality $Ge_{1-x}Sn_x$

https://doi.org/10.1021/acsaelm.3c00112
ACS Appl. Electron. Mater. 2023, 5, 2268−2275

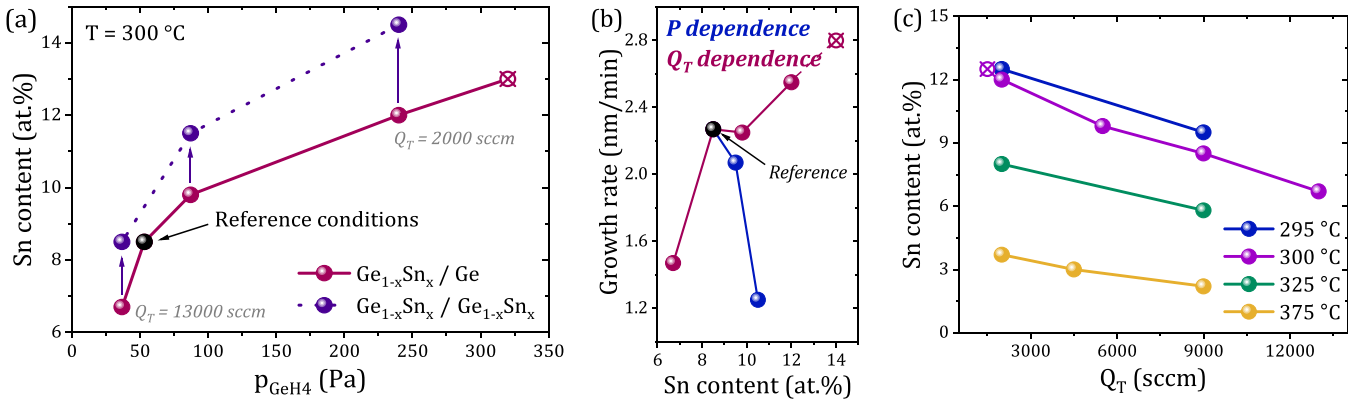

Figure 2. (a) Sn content incorporation at 300 °C as a function of the partial pressure of GeH_4 for different total N_2 flows grown onto Ge (pink) and $Ge_{1-x}Sn_x$ (purple) buffer layers. The black point represents the "reference" growth conditions, and the cross-white symbols correspond to samples that show Sn segregation on the surface. (b) Growth rate as a function of the Sn content corresponding to changes in the reactor pressure and total N_2 flow. (c) Summary of the Sn content as a function of total carrier gas flow at different growth temperatures showing similar behavior.

layers. Using GeH_4 instead of Ge_2H_6, the amount of GeH_3 reactive molecules available in the reactor is reduced by half for the same gas flow, and considering the activation energy of 1.3 eV for GeH_4, higher than 0.7 eV for Ge_2H_6,[24] the GeH_4 gas flow was increased by a factor of 4, in-line with Hartmann et al.'s[30] findings. The used growth parameters of partial pressure ratio p_{GeH4}/p_{SnCl4} = 1100, reactor pressure of P_{react} = 60 mbar, and total gas flow Q_{total} = 9000 sccm are further called "reference" growth conditions.

The stoichiometry, thickness, and crystal quality of the epitaxial layers were extracted by fitting the Rutherford backscattering spectra (RBS) taken at random and channeling alignment using a Tandetron accelerator with 1.4 MeV He^+ ions at a backscattering angle of 170°. The crystal orientation and the strain build-up in the films were determined by X-ray diffraction (XRD) and reciprocal space mapping (RSM), respectively, while the crystal quality was verified by transmission electron microscopy (TEM) imaging. Finally, temperature-dependent photoluminescence (PL) spectra and electronic band structure calculations were performed to address the suitability of the $Ge_{1-x}Sn_x$ heterostructures for specific applications.

RESULTS AND DISCUSSION

Reference Growth Conditions - Temperature Dependence. The classical pathway toward high Sn content layers is the decrease of the process temperature while keeping all other growth parameters constant. A set of wafers has been grown on 300 nm-thick Ge/Si (001) substrates at temperatures ranging between 295 and 400 °C, using the reference growth conditions given above. The layer's thickness and stoichiometry were obtained by fitting the RBS random spectra as shown in Figure 1a. For clarity, only the energy region between 0.9 and 1.3 MeV, corresponding to the Ge and Sn signals in the $Ge_{1-x}Sn_x$ layers is shown, while a full RBS spectrum is exemplified in the inset. The plateaus visible at a backscattered ion energy of ∼1.2 MeV are evidence of uniform depth distribution of the Sn atoms. The Sn concentration increases from about 1 at. % up to 9.5 at. % by decreasing the growth temperature from 400 to 295 °C, as shown in Figure 1b (left scale, top panel). At a lower temperature of 290 °C, the Sn content reaches ∼10 at. % and the wafer presents a mirror-like surface, but isolated Sn segregation occurs. Further temperature decrease leads to a large Sn segregation, as illustrated in the scanning electron microscope (SEM) and optical images (inset) presented in Figure 1d,e, showing a mirror-like and a Sn segregation surface, respectively. The growth rate determined from the thickness extracted from the RBS fitting (Figure 1b) varies strongly with the temperature from ∼13 nm/min at 400 °C to 2 nm/min at 295 °C. This behavior for different process temperatures is in perfect agreement with the literature reports.[30−32]

The crystalline quality of the $Ge_{1-x}Sn_x$ alloy is visible from the minimum channeling yield χ_{min} (Figure 1b, bottom panel), defined as the ratio of intensities between channeling and random RBS spectra (Figure 1a) measured directly behind the surface peak. In agreement with previous reports,[33,34] the low $\chi_{min} \leq 6\%$ for all samples indicates the high $Ge_{1-x}Sn_x$ single-crystalline quality and high substitutability of the Sn atoms. The opposite is obtained in the samples where Sn segregation occurs, characterized by high values of χ_{min} and nonuniform plateau (Figure 1e).

The results are confirmed by the symmetric XRD spectra taken along the (004) plane (Figure 1c) where the $Ge_{1-x}Sn_x$ diffraction peaks systematically shift away from the Ge peak toward lower 2θ angles, as a result of the increasing out-of-plane lattice constant due to higher Sn incorporation and correspondingly increased compressive biaxial strain. From the position of the $Ge_{1-x}Sn_x$ peak in the RSMs, and using Vegard's law with a bowing parameter of 0.04, the Sn content was extracted (yellow symbols in Figure 1b), showing an excellent agreement with RBS fitting. All $Ge_{1-x}Sn_x$ layers grown here are fully compressively strained (pseudomorphic growth), evidenced from the same in-plane lattice constant with the Ge buffer layer, which is slightly tensile strained (0.15%) (see Figure S1 in the Supporting Information (SI) file). The build-up of tetragonal elastic strain in the $Ge_{1-x}Sn_x$ alloy for different Sn compositions changes from almost a cubic lattice (∼0% strain) at 400 °C to −1.25% compressive biaxial strain for $Ge_{0.905}Sn_{0.095}$ layer growth at 295 °C.

Isothermal Growth Conditions. The typical approaches for tuning the alloy composition[21,22,30,35,36] at constant process temperature are performed by changing the precursors' flow or the reactor pressure. Starting from the reference growth conditions at 300 °C, the decrease/increase in the GeH_4 and $SnCl_4$ partial pressures through the direct control of the flux of these precursors results in small changes of the Sn incorporation, giving a maximum Sn concentration of 9.0−9.5 at. %, compared to the 8.5 at. % Sn obtained under the reference growth conditions (Figure S2a,b of the SI). Another way to increase the Sn incorporation is to change the reactor pressure while keeping the total flow and the precursors flow constants as the "reference" values, meaning a constant p_{GeH4}/

https://doi.org/10.1021/acsaelm.3c00112
ACS Appl. Electron. Mater. 2023, 5, 2268−2275

p_{SnCl4} ratio. The reactor pressure change between 60 and 200 mbar translating into a $SnCl_4$ partial pressure between 0.05 (reference growth conditions) and 0.16 Pa results in a maximum Sn incorporation of 10.5 at. % at the highest reactor pressure value (Figure S2c of the SI).

For some electronic devices like nanowire MOSFETs where the nanowire patterning relaxes the strain in the $Ge_{1-x}Sn_x$ layer,[5] an Sn content around 10 at. % might be sufficient, but larger Sn contents are still required to reach a strongly direct band gap for photonic applications like light emitter or lasers. The next growth parameter to study, which may increase the Sn incorporation, is the N_2 carrier gas flow. Both parameters, increasing the total pressure or decreasing the N_2 flow rate, have similar effects. The precursor partial pressures are proportionally increased with the factor of pressure increase or N_2 flow reduction. The gas flow rate decreases, i.e., the retention time of the reactive precursors in the reactor increases for both cases. Consequently, the amount of GeH_x radicals on the surface will increase as well.

The total gas flow in the reactor, Q_T, (Figure 2a) is adjusted by tuning the N_2 carrier gas flow at constant total pressure and a ratio p_{GeH4}/p_{SnCl4} = 1100 ("reference" growth condition). In this way, the gas flow rate and the partial pressure of the precursors change, and therefore the gas phase reactions are modified, with an impact on the surface kinetics. Keeping the growth temperature of 300 °C, the decrease of Q_T from 13,000 to 2000 sccm greatly increases the Sn content from 6.5 to 12 at. %. Since the precursor fluxes have been kept constant, their partial pressures increase by a factor of 6.5. A further decrease in the N_2 flow leads to a $SnCl_4$ partial pressure of 0.3 Pa at which Sn segregation takes place (empty symbol, Figure 2a).

The growth rates corresponding to the pressure and total gas flow variations are shown in Figure 2b. Interestingly, the $Ge_{1-x}Sn_x$ growth rate has a completely opposite behavior: while it decreases with the increasing Sn content under pressure variation, the highest growth rate is obtained for the larger Sn incorporation by the N_2 flow change. Moreover, the same growth rate of ∼2.6−2.8 nm/min is obtained also by changing the $SnCl_4$ flow (Figure S2b of SI); however, it offers only ∼9 at. % Sn incorporation compared to 12 at. % Sn in the case of N_2 flow tuning. These important observations make the N_2 flow change method very attractive for high Sn content device epitaxy.

To summarize the data at different growth temperatures, the plot in Figure 2c shows the relation between the Sn content in the $Ge_{1-x}Sn_x$ alloy and the total gas flow at different process temperatures. It becomes clear that increasing the $SnCl_4$ partial pressure through the decrease of the total flow stimulates the Sn incorporation in the Ge lattice regardless of the process temperature. This plot shows that a large stoichiometry tuning in $Ge_{1-x}Sn_x$ multilayers can be obtained by isothermal epitaxial growth only via total carrier flow.

The above observation (pink curve in Figure 2a) refers to lattice-matched $Ge_{1-x}Sn_x$ epitaxy directly on Ge buffer. However, if under the same growth conditions, the film is grown beyond the critical thickness, the bottom $Ge_{1-x}Sn_x$ relaxes, offering a larger lattice constant, reduced surface strain, and increased surface mobility of the adatoms. These lead to a considerably larger Sn content incorporation into the subsequent $Ge_{1-x}Sn_x$ epitaxial layer[37−39] (purple curve in Figure 2a). Under a constant total flow of 2000 sccm and increasing the growth time, it is possible to increase the Sn concentration from 11.5 to 14.5 at. %. Such layers were successfully used as optical active media for $Ge_{1-x}Sn_x$ laser fabrication,[1] but the method cannot offer controlled thickness and Sn content demanding, for example, in quantum well heterostructures.

Isothermal Growth of $Ge_{1-x}Sn_x$ Heterostructures for Electronic and Photonic Device Applications. Using the knowledge gained, different heterostructures have been grown showing the wide possibilities offered by the N_2 gas flow change method. The aim was to realize $Ge_{1-x}Sn_x$ isothermal heterostructures where the Sn content is varied according to the application design requirements. Such heterostructures, discussed below, are illustrated in Table 1. In all cases, the same process temperature of 300 °C, pressure of 60 mbar, and p_{GeH4}/p_{SnCl4} = 1100, as for the reference sample, were used.

Table 1. Summary of the Growth Parameters such as Total Carrier Gas (Q_T), Sn Content, Thickness (d), and Precursors Flow of the Heterostructures Shown in Figures 3 and 4[a]

		Q_T (sccm)	Sn content (at. %)	d (nm)	$SnCl_4$ flow (sscm)	GeH_4 flow (sscm)
Structure I	top layer	2000	15	60	8	1000
	bottom layer	9000	12	100		
Structure II	top layer	13,000	8	60	6	800
	middle layer	9000	9	75		
	bottom layer	2000	11	90		
Structure III	5 × MQW				6	800
	wells	2000	15.5	30		
	barriers	15,000	9.5	12		
	buffer layer	9000	13	40		
	bottom layer	2000	12	310		

[a]The "bottom layer" corresponds to the layer grown on the Ge buffer layer while the "top layer" is the last grown layer.

Structure I was designed by selecting the optimal values of the Sn and Ge flux that enhance the incorporation of Sn into the alloy (Figure S2 of SI) while the N_2 flow was decreased from 9000 to 2000 sccm. The N_2 gas flow was here intentionally continuously changed, leading to a Sn gradient change over ∼40 nm, allowing continuous epitaxial growth without additional strain relaxation as indicated by the RSM spectrum overlapping the TEM micrograph in Figure 3a. In addition, as the thickness of the top layer remains below the critical thickness, the bottom layer is partially relaxed, while the top layer is strained to the first layer. As a result, the first 100 nm-thick layer has 12 at. % of Sn, higher than the sample grown under the "reference" growth conditions with 8.5 at. %. Note that the $Ge_{0.85}Sn_{0.15}$ top layer, at p_{GeH4} = 300 Pa, is epitaxially grown on $Ge_{0.88}Sn_{0.12}$, while Sn segregation appears by direct growth on Ge buffer under similar growth conditions (empty pink symbol in Figure 2a). Structure I design is an upgraded heterostructure for vertical MOSFET devices and CMOS invertors, as recently experimentally demonstrated by Liu et al.[5,40] The patterning into nanowires (NWs) with diameters below 100 nm results in elastic strain relaxation, offering direct band gap $Ge_{1-x}Sn_x$ semiconductors with a large separation between the Γ- and L-valleys. NW MOSFET devices, as sketched in Figure 3b, fully benefit from the high mobility of Γ-electrons in direct band gap $Ge_{1-x}Sn_x$ compared to that of L-electrons in the indirect Ge semiconductor, boosting the n-type MOSFET devices. The calculated electron

https://doi.org/10.1021/acsaelm.3c00112
ACS Appl. Electron. Mater. 2023, 5, 2268−2275

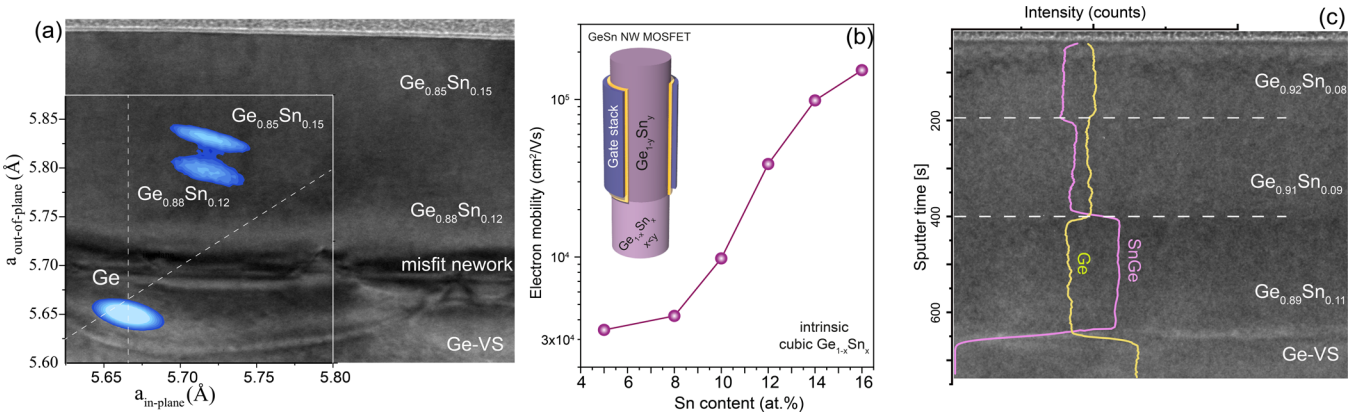

Figure 3. (a) Cross-sectional TEM micrographs of $Ge_{0.85}Sn_{0.15}/Ge_{0.88}Sn_{0.12}/Ge$ buffer heterostructure overlapped with the RSM spectrum. (b) Calculated electron mobility vs Sn content. Inset: sketch of a vertical $Ge_{1-x}Sn_x$ NW MOSFET. (c) Cross-sectional TEM micrograph of structure II grown at 300 °C varying the N_2 carrier gas flow, overlapped with SIMS profile of an inverse−step Sn content $Ge_{0.92}Sn_{0.08}/Ge_{0.91}Sn_{0.09}/Ge_{0.89}Sn_{0.11}/Ge$ heterostructure. The Ge intensity is artificially reduced by 50% for better comparison. Some more data are given in the SI, Figures S3 and S4.

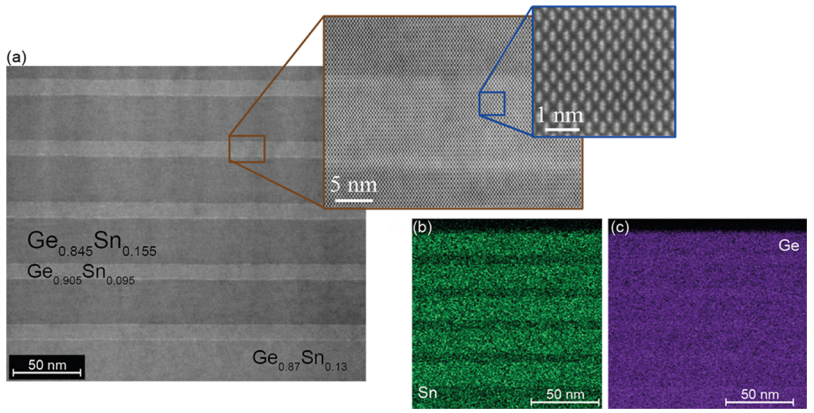

Figure 4. (a) High-resolution TEM and (b, c) energy-dispersive X-ray spectroscopy high-angle annular dark-field (EDS-HAADF) micrographs of a strained $Ge_{0.845}Sn_{0.155}/Ge_{0.905}Sn_{0.095}$ multiple QW heterostructure (structure III). Some more data are given in the SI, Figures S3 and S4.

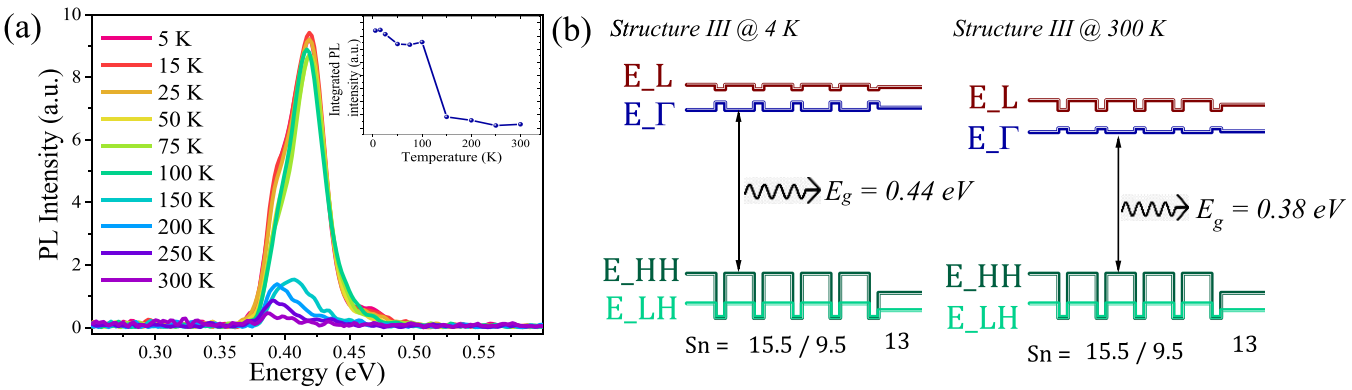

Figure 5. (a) Temperature-dependent PL spectra and (b) electronic band structure calculation at 4 and 300 K for structure III.

mobility versus Sn concentration for tetragonal and cubic $Ge_{1-x}Sn_x$ alloys is presented in Figure 3b. For the electron mobility calculation, the conventional, relaxation time-based calculation, using the 8-band k.p model for Γ-electrons and for holes, and effective-mass (with non-parabolicity) model for L-valley electrons was used.[41−43]

Aiming for ultralow-power electronics, tunneling field-effect transistors (TFETs) were recently investigated.[44,45] The small effective masses for both holes and electrons[46] in $Ge_{1-x}Sn_x$ alloys and the lower band gap make their use in TFET devices very advantageous. For this purpose, a $Ge_{1-x}Sn_x$-based heterostructure design with decreasing Sn content per layer (inverse-step) is proposed in Figure 3c (structure II). The Sn and Ge elemental secondary ion mass spectrometry (SIMS) spectra overlapping a TEM micrograph indicate the $Ge_{0.89}Sn_{0.11}$ source (bottom layer) followed by the $Ge_{0.91}Sn_{0.09}$ channel (middle layer) and the larger band gap $Ge_{0.92}Sn_{0.08}$ drain (top layer). This multilayer structure was isothermally grown at 300 °C, under the "reference" GeH_4 and

https://doi.org/10.1021/acsaelm.3c00112
ACS Appl. Electron. Mater. 2023, 5, 2268−2275

$SnCl_4$ flux, decreasing the Sn concentration only by increasing the total flow, i.e., Q_T as indicated in Table 1.

Finally, the combination of growth methodologies used for structures I and II offer an isothermal multiple quantum well (MQW) heterostructure as shown in structure III (Figure 4). Such a design dramatically reduces the injection current threshold by the carrier confinement, being a pathway for the development of $Ge_{1-x}Sn_x$ light sources.[15,47] Fully strained 5× $Ge_{0.845}Sn_{0.155}/Ge_{0.905}Sn_{0.095}$ QWs were grown on a 40 nm-thick $Ge_{0.87}Sn_{0.13}$ buffer layer on an almost relaxed $Ge_{1-x}Sn_x$ bottom layer. The TEM/EDS-HAADF micrographs show the very high crystallinity of the epitaxial stack without interface defects between different $Ge_{1-x}Sn_x$ layers. Additional data such as XRD diffractograms, RSM scans, SIMS profiles, and HR-TEM micrographs are available in Figures S3 and S4 of the SI.

The temperature-dependent PL measurements for the structure III are presented in Figure 5a. The PL signal comes from the layers with the lowest band gap energy, here the 15.5 at. % Sn content wells (Table 1). If the temperature decreases, the PL peak position shifts toward higher energy, and the intensity of the PL signal increases, as expected due to the nature of the temperature-dependent band gap.[1] A clear emission change is visible at 150 K where the intensity decreases abruptly (inset in Figure 5a). If the temperature increases, the conduction band offset between the wells and the barriers reduces and the electrons can escape from the well, resulting in an inefficient confinement effect. Consequently, the MQW behaves similarly to a bulk layer. The PL emission data at both 4 and 300 K are in excellent agreement with the electronic band structure calculation[48] performed using the Sn and strain profiles determined by RBS and XRD measurements (Figure 5b).

CONCLUSIONS

A simple technical epitaxial growth approach that allows isothermal epitaxy of $Ge_{1-x}Sn_x$ semiconductors heterostructures with different compositions has been presented. The simplest method to largely vary Sn incorporation in the Ge lattice is the tuning of the N_2 flow used as a carrier gas, while keeping the process temperature, deposition pressure, and precursor fluxes constant. Three heterostructures of high-quality $Ge_{1-x}Sn_x$ layers were grown with the desired Sn profiles, including the inverse-step Sn content of up to 15 at. % Sn and QW structures targeting different applications such as vertical NW-FETs, tunneling FETs, and mid-IR light emitters. While the growth parameters optimization can be required for specific heterostructure designs, the results presented here prove the suitability of GeH_4 as a cheaper, stable, and easier-to-handle precursor for state-of-the-art high Sn content $Ge_{1-x}Sn_x$ heterostructures.

ASSOCIATED CONTENT

Supporting Information

The Supporting Information is available free of charge at https://pubs.acs.org/doi/10.1021/acsaelm.3c00112.

Structural characterization of $Ge_{1-x}Sn_x$ layers grown at different process temperatures; Sn content and growth rate depending on growth parameters; structural characterization of isothermal heterostructures (PDF)

AUTHOR INFORMATION

Corresponding Author

Omar Concepción − *Peter Gruenberg Institute 9 (PGI-9), Forschungszentrum Juelich, 52428 Juelich, Germany;* orcid.org/0000-0001-8197-7523; Email: o.diaz@fz-juelich.de

Authors

Nicolaj B. Søgaard − *Interdisciplinary Nanoscience Center (iNANO), Aarhus University, 8000 Aarhus, Denmark;* orcid.org/0000-0002-6718-0910

Jin-Hee Bae − *Peter Gruenberg Institute 9 (PGI-9), Forschungszentrum Juelich, 52428 Juelich, Germany*

Yuji Yamamoto − *IHP - Leibniz Institut für innovative Mikroelektronik, 15236 Frankfurt (Oder), Germany*

Andreas T. Tiedemann − *Peter Gruenberg Institute 9 (PGI-9), Forschungszentrum Juelich, 52428 Juelich, Germany*

Zoran Ikonic − *Pollard Institute, School of Electronic and Electrical Engineering, University of Leeds, Leeds LS2 9JT, United Kingdom*

Giovanni Capellini − *IHP - Leibniz Institut für innovative Mikroelektronik, 15236 Frankfurt (Oder), Germany; Dipartimento di Scienze, Università Roma Tre, 00146 Roma, Italy*

Qing-Tai Zhao − *Peter Gruenberg Institute 9 (PGI-9), Forschungszentrum Juelich, 52428 Juelich, Germany;* orcid.org/0000-0002-2794-2757

Detlev Grützmacher − *Peter Gruenberg Institute 9 (PGI-9), Forschungszentrum Juelich, 52428 Juelich, Germany*

Dan Buca − *Peter Gruenberg Institute 9 (PGI-9), Forschungszentrum Juelich, 52428 Juelich, Germany*

Complete contact information is available at: https://pubs.acs.org/10.1021/acsaelm.3c00112

Author Contributions

The manuscript was written through the contributions of all authors. All authors have given approval for the final version of the manuscript.

Funding

The authors acknowledge financial support by Deutsche Forschungsgemeinschaft (DFG) under grant no. CA 1474/2-2 "SiGeSn Laser for Silicon Photonics" and to the European Union support via the Project Laststep.

Notes

The authors declare no competing financial interest.

ACKNOWLEDGMENTS

The authors would like to thank to Patric Bernardy and Karl-Heinz Deussen for their experimental and technical support.

ABBREVIATIONS

NIR/MIR, near-/mid-infrared; SOC, spin−orbit coupling; QW, quantum well; MOSFET, metal oxide semiconductor field-effect transistor; RP-CVD, reduced-pressure chemical vapor deposition; VS, virtual substrate; RBS, Rutherford backscattering spectroscopy; XRD, X-ray diffraction; RSM, reciprocal space mapping; TEM, transmission electron microscopy; PL, photoluminescence; SI, Supporting Information; NW, nanowire; TFET, tunneling field-effect transistor; SIMS, secondary ion mass spectrometry; MQW, multiple quantum well; EDS-HAADF, energy-dispersive X-ray spectroscopy high-angle annular dark-field

https://doi.org/10.1021/acsaelm.3c00112
ACS Appl. Electron. Mater. 2023, 5, 2268−2275

REFERENCES

(1) Wirths, S.; Geiger, R.; Von Den Driesch, N.; Mussler, G.; Stoica, T.; Mantl, S.; Ikonic, Z.; Luysberg, M.; Chiussi, S.; Hartmann, J. M.; Sigg, H.; Faist, J.; Buca, D.; Grützmacher, D. Lasing in Direct-Bandgap GeSn Alloy Grown on Si. *Nat. Photonics* **2015**, *9*, 88−92.

(2) Chrétien, J.; Thai, Q. M.; Frauenrath, M.; Casiez, L.; Chelnokov, A.; Reboud, V.; Hartmann, J. M.; El Kurdi, M.; Pauc, N.; Calvo, V. Room Temperature Optically Pumped GeSn Microdisk Lasers. *Appl. Phys. Lett.* **2022**, *120*, No. 051107.

(3) Zhou, Y.; Ojo, S.; Wu, C.-W.; Miao, Y.; Tran, H.; Grant, J. M.; Abernathy, G.; Amoah, S.; Bass, J.; Salamo, G.; Du, W.; Chang, G.-E.; Liu, J.; Margetis, J.; Tolle, J.; Zhang, Y.-H.; Sun, G.; Soref, R. A.; Li, B.; Yu, S.-Q. Electrically Injected GeSn Lasers with Peak Wavelength up to 2.7 Mm. *Photonics Res.* **2022**, *10*, 222.

(4) Talamas Simola, E.; Kiyek, V.; Ballabio, A.; Schlykow, V.; Frigerio, J.; Zucchetti, C.; De Iacovo, A.; Colace, L.; Yamamoto, Y.; Capellini, G.; Grützmacher, D.; Buca, D.; Isella, G. CMOS-Compatible Bias-Tunable Dual-Band Detector Based on GeSn/Ge/Si Coupled Photodiodes. *ACS Photonics* **2021**, *8*, 2166−2173.

(5) Liu, M.; Yang, D.; Shkurmanov, A.; Bae, J. H.; Schlykow, V.; Hartmann, J.-M.; Ikonic, Z.; Baerwolf, F.; Costina, I.; Mai, A.; Knoch, J.; Grützmacher, D.; Buca, D.; Zhao, Q.-T. Epitaxial GeSn/Ge Vertical Nanowires for p-Type Field-Effect Transistors with Enhanced Performance. *ACS Appl. Nano Mater.* **2021**, *4*, 94−101.

(6) Spirito, D.; von den Driesch, N.; Manganelli, C. L.; Zoellner, M. H.; Corley-Wiciak, A. A.; Ikonic, Z.; Stoica, T.; Grützmacher, D.; Buca, D.; Capellini, G. Thermoelectric Efficiency of Epitaxial GeSn Alloys for Integrated Si-Based Applications: Assessing the Lattice Thermal Conductivity by Raman Thermometry. *ACS Appl. Energy Mater.* **2021**, *4*, 7385−7392.

(7) Marchionni, A.; Zucchetti, C.; Ciccacci, F.; Finazzi, M.; Funk, H. S.; Schwarz, D.; Oehme, M.; Schulze, J.; Bottegoni, F. Inverse Spin-Hall Effect in GeSn. *Appl. Phys. Lett.* **2021**, *118*, 212402.

(8) Chen, Q.; Wu, S.; Zhang, L.; Fan, W.; Tan, C. S. Simulation of High-Efficiency Resonant-Cavity-Enhanced GeSn Single-Photon Avalanche Photodiodes for Sensing and Optical Quantum Applications. *IEEE Sens. J.* **2021**, *21*, 14789−14798.

(9) Jirovec, D.; Hofmann, A.; Ballabio, A.; Mutter, P. M.; Tavani, G.; Botifoll, M.; Crippa, A.; Kukucka, J.; Sagi, O.; Martins, F.; Saez-Mollejo, J.; Prieto, I.; Borovkov, M.; Arbiol, J.; Chrastina, D.; Isella, G.; Katsaros, G. A Singlet-Triplet Hole Spin Qubit in Planar Ge. *Nat. Mater.* **2021**, *20*, 1106−1112.

(10) Hendrickx, N. W.; Franke, D. P.; Sammak, A.; Scappucci, G.; Veldhorst, M. Fast Two-Qubit Logic with Holes in Germanium. *Nature* **2020**, *577*, 487−491.

(11) Tai, C.-T.; Chiu, P.-Y.; Liu, C.-Y.; Kao, H.-S.; Harris, C. T.; Lu, T.-M.; Hsieh, C.-T.; Chang, S.-W.; Li, J.-Y.; Tai, C.-T.; Chiu, P.-Y.; Liu, C.-Y.; Kao, H.-S.; Li, J.-Y.; Harris, C. T.; Lu, T.-M.; Hsieh, C.-T.; Chang, S.-W. Strain Effects on Rashba Spin-Orbit Coupling of 2D Hole Gases in GeSn/Ge Heterostructures. *Adv. Mater.* **2021**, *33*, No. 2007862.

(12) Grützmacher, D.; Concepción, O.; Zhao, Q.-T.; Buca, D. Si−Ge−Sn Alloys Grown by Chemical Vapour Deposition: A Versatile Material for Photonics, Electronics, and Thermoelectrics. *Appl. Phys. A: Mater. Sci. Process.* **2023**, *129*, 1−10.

(13) von den Driesch, N.; Wirths, S.; Troitsch, R.; Mussler, G.; Breuer, U.; Moutanabbir, O.; Grützmacher, D.; Buca, D. Thermally Activated Diffusion and Lattice Relaxation in (Si)GeSn Materials. *Phys. Rev. Mater.* **2020**, *4*, No. 033604.

(14) Jahandar, P.; Weisshaupt, D.; Colston, G.; Allred, P.; Schulze, J.; Myronov, M. The Effect of Ge Precursor on the Heteroepitaxy of Ge 1− x Sn x Epilayers on a Si (001) Substrate. *Semicond. Sci. Technol.* **2018**, *33*, No. 034003.

(15) Stange, D.; von den Driesch, N.; Rainko, D.; Roesgaard, S.; Povstugar, I.; Hartmann, J.-M.; Stoica, T.; Ikonic, Z.; Mantl, S.; Grützmacher, D.; Buca, D. Short-Wave Infrared LEDs from GeSn/SiGeSn Multiple Quantum Wells. *Optica* **2017**, *4*, 185.

(16) von den Driesch, N.; Stange, D.; Rainko, D.; Povstugar, I.; Zaumseil, P.; Capellini, G.; Schröder, T.; Denneulin, T.; Ikonic, Z.; Hartmann, J.-M.; Sigg, H.; Mantl, S.; Grützmacher, D.; Buca, D. Advanced GeSn/SiGeSn Group IV Heterostructure Lasers. *Adv. Sci.* **2018**, DOI: 10.1002/advs.201700955.

(17) Assali, S.; Attiaoui, A.; Del Vecchio, P.; Mukherjee, S.; Nicolas, J.; Moutanabbir, O. *A Light-Hole Quantum Well on Silicon*. 2021.

(18) Von Den Driesch, N.; Stange, D.; Wirths, S.; Mussler, G.; Holländer, B.; Ikonic, Z.; Hartmann, J. M.; Stoica, T.; Mantl, S.; Grützmacher, D.; Buca, D. Direct Bandgap Group IV Epitaxy on Si for Laser Applications. *Chem. Mater.* **2015**, *27*, 4693−4702.

(19) Gencarelli, F.; Vincent, B.; Demeulemeester, J.; Vantomme, A.; Moussa, A.; Franquet, A.; Kumar, A.; Bender, H.; Meersschaut, J.; Vandervorst, W.; Loo, R.; Caymax, M.; Temst, K.; Heyns, M. Crystalline Properties and Strain Relaxation Mechanism of CVD Grown GeSn. *ECS J. Solid State Sci. Technol.* **2013**, *2*, P134−P137.

(20) Gencarelli, F.; Shimura, Y.; Kumar, A.; Vincent, B.; Moussa, A.; Vanhaeren, D.; Richard, O.; Bender, H.; Vandervorst, W.; Caymax, M.; Loo, R.; Heyns, M. Amorphous Inclusions during Ge and GeSn Epitaxial Growth via Chemical Vapor Deposition. *Thin Solid Films* **2015**, *590*, 163−169.

(21) Loo, R.; Shimura, Y.; Ike, S.; Vohra, A.; Stoica, T.; Stange, D.; Buca, D.; Kohen, D.; Margetis, J.; Tolle, J. Epitaxial GeSn: Impact of Process Conditions on Material Quality. *Semicond. Sci. Technol.* **2018**, *33*, 114010.

(22) Jahandar, P.; Weisshaupt, D.; Colston, G.; Allred, P.; Schulze, J.; Myronov, M. The Effect of Ge Precursor on the Heteroepitaxy of Ge1−xSnx Epilayers on a Si (001) Substrate. *Semicond. Sci. Technol.* **2018**, *33*, No. 034003.

(23) Grant, P. C.; Dou, W.; Alharthi, B.; Grant, J. M.; Mosleh, A.; Du, W.; Li, B.; Mortazavi, M.; Naseem, H. A.; Yu, S.-Q. Comparison Study of the Low Temperature Growth of Dilute GeSn and Ge. *J. Vac. Sci. Technol., B: Nanotechnol. Microelectron.: Mater., Process., Meas., Phenom.* **2017**, *35*, No. 061204.

(24) Wirths, S.; Buca, D.; Tiedemann, A. T.; Holländer, B.; Bernardy, P.; Stoica, T.; Grützmacher, D.; Mantl, S. Epitaxial Growth of Ge 1-x Sn x by Reduced Pressure CVD Using SnCl 4 and Ge 2 H 6. *ECS Trans.* **2013**, *50*, 885−893.

(25) Grützmacher, D. A.; Sedgwick, T. O.; Powell, A.; Tejwani, M.; Iyer, S. S.; Cotte, J.; Cardone, F. Ge Segregation in SiGe/Si Heterostructures and Its Dependence on Deposition Technique and Growth Atmosphere. *Appl. Phys. Lett.* **1993**, *63*, 2531−2533.

(26) Sedgwick, T. O.; Agnello, P. D.; Grützmacher, D. A. Effects of Trace Surface Oxidation in Low Temperature Epitaxy Grown from Dichlorosilane. *J. Electrochem. Soc.* **1993**, *140*, 3684−3688.

(27) Gates, S. M.; Greenlief, C. M.; Beach, D. B. Decomposition Mechanisms of SiHx Species on Si(100)-(2×1) for X=2, 3, and 4. *J. Chem. Phys.* **1990**, *93*, 7493−7503.

(28) Yamamoto, Y.; Zaumseil, P.; Arguirov, T.; Kittler, M.; Tillack, B. Low Threading Dislocation Density Ge Deposited on Si (1 0 0) Using RPCVD. *Solid-State Electron.* **2011**, *60*, 2−6.

(29) von den Driesch, N.; Stange, D.; Wirths, S.; Rainko, D.; Povstugar, I.; Savenko, A.; Breuer, U.; Geiger, R.; Sigg, H.; Ikonic, Z.; Hartmann, J.; Grützmacher, D.; Mantl, S.; Buca, D. SiGeSn Ternaries for Efficient Group IV Heterostructure Light Emitters. *Small* **2017**, *13*, No. 1603321.

(30) Hartmann, J.-M.; Frauenrath, M.; Richy, J. Epitaxy of Pseudomorphic GeSn Layers with Germane (GeH4) or Digermane (Ge2H6) as Ge Precursors and Tin Tetrachloride (SnCl4) as the Sn Precursor. *ECS Trans.* **2020**, *98*, 225−238.

(31) Aubin, J.; Hartmann, J. M. GeSn Growth Kinetics in Reduced Pressure Chemical Vapor Deposition from Ge2H6 and SnCl4. *J. Cryst. Growth* **2018**, *482*, 30−35.

(32) Grant, P. C.; Dou, W.; Alharthi, B.; Grant, J. M.; Tran, H.; Abernathy, G.; Mosleh, A.; Du, W.; Li, B.; Mortazavi, M.; Naseem, H. A.; Yu, S.-Q. UHV-CVD Growth of High Quality GeSn Using SnCl4: From Material Growth Development to Prototype Devices. *Opt. Mater. Express* **2019**, *9*, 3277.

(33) Bhargava, N.; Coppinger, M.; Prakash Gupta, J.; Wielunski, L.; Kolodzey, J. Lattice Constant and Substitutional Composition of

https://doi.org/10.1021/acsaelm.3c00112
ACS Appl. Electron. Mater. 2023, 5, 2268−2275

GeSn Alloys Grown by Molecular Beam Epitaxy. *Appl. Phys. Lett.* **2013**, *103*, No. 041908.
(34) Margetis, J.; Ghetmiri, S. A.; Du, W.; Conley, B. R.; Mosleh, A.; Soref, R.; Sun, G.; Domulevicz, L.; Naseem, H. A.; Yu, S.-Q.; Tolle, J. Growth and Characterization of Epitaxial Ge1-XSnx Alloys and Heterostructures Using a Commercial CVD System. *ECS Trans.* **2014**, *64*, 711−720.
(35) Grant, J.; Abernathy, G.; Olorunsola, O.; Ojo, S.; Amoah, S.; Wanglia, E.; Saha, S. K.; Sabbar, A.; Du, W.; Alher, M.; Li, B.-H.; Yu, S.-Q. Growth of Pseudomorphic GeSn at Low Pressure with Sn Composition of 16.7%. *Materials* **2021**, *14*, 7637.
(36) Margetis, J.; Yu, S.-Q.; Li, B.; Tolle, J. Chemistry and Kinetics Governing Hydride/Chloride Chemical Vapor Deposition of Epitaxial Ge 1−x Sn X. *J. Vac. Sci. Technol., A* **2019**, *37*, No. 021508.
(37) Al-Kabi, S.; Ghetmiri, S. A.; Margetis, J.; Du, W.; Mosleh, A.; Dou, W.; Sun, G.; Soref, R. A.; Tolle, J.; Li, B.; Mortazavi, M.; Naseem, H. A.; Yu, S. Q. Study of High-Quality GeSn Alloys Grown by Chemical Vapor Deposition towards Mid-Infrared Applications. *J. Electron. Mater.* **2016**, *45*, 6251−6257.
(38) Margetis, J.; Mosleh, A.; Al-Kabi, S.; Ghetmiri, S. A.; Du, W.; Dou, W.; Benamara, M.; Li, B.; Mortazavi, M.; Naseem, H. A.; Yu, S. Q.; Tolle, J. Study of Low-Defect and Strain-Relaxed GeSn Growth via Reduced Pressure CVD in H2 and N2 Carrier Gas. *J. Cryst. Growth* **2017**, *463*, 128−133.
(39) Dou, W.; Benamara, M.; Mosleh, A.; Margetis, J.; Grant, P.; Zhou, Y.; Al-Kabi, S.; Du, W.; Tolle, J.; Li, B.; Mortazavi, M.; Yu, S. Q. Investigation of GeSn Strain Relaxation and Spontaneous Composition Gradient for Low-Defect and High-Sn Alloy Growth. *Sci. Rep.* **2018**, *8*, 1−11.
(40) Liu, M.; Junk, Y.; Han, Y.; Yang, D.; Bae, J. H.; Frauenrath, M.; Hartmann, J.-M.; Ikonic, Z.; Bärwolf, F.; Mai, A.; Grützmacher, D.; Knoch, J.; Buca, D.; Zhao, Q.-T. Vertical GeSn Nanowire MOSFETs for CMOS beyond Silicon. *Commun. Eng.* **2023**, *2*, 1−9.
(41) Jacoboni, C.; Reggiani, L. The Monte Carlo Method for the Solution of Charge Transport in Semiconductors with Applications to Covalent Materials. *Rev. Mod. Phys.* **1983**, *55*, 645.
(42) Fu, Y.; Joelsson, K. B.; Grahn, K. J.; Ni, W.-X.; Hansson, G. V.; Willander, M. *Hall Factor in Strained P-Type Doped Si 1x Ge x Alloy*. 1996.
(43) Schulte-Braucks, C.; Glass, S.; Hofmann, E.; Stange, D.; von den Driesch, N.; Hartmann, J. M.; Ikonic, Z.; Zhao, Q. T.; Buca, D.; Mantl, S. Process Modules for GeSn Nanoelectronics with High Sn-Contents. *Solid-State Electron.* **2017**, *128*, 54−59.
(44) Yang, Y.; Han, G.; Guo, P.; Wang, W.; Gong, X.; Wang, L.; Low, K. L.; Yeo, Y. Germanium–Tin P-Channel Tunneling Field-Effect Transistor: Device Design and Technology Demonstration. *IEEE Trans. Electron. Devices* **2013**, *60*, 4048−4056.
(45) Wirths, S.; Tiedemann, A. T.; Ikonic, Z.; Harrison, P.; Holländer, B.; Stoica, T.; Mussler, G.; Myronov, M.; Hartmann, J. M.; Grützmacher, D.; Buca, D.; Mantl, S. Band Engineering and Growth of Tensile Strained Ge/(Si)GeSn Heterostructures for Tunnel Field Effect Transistors. *Appl. Phys. Lett.* **2013**, *102*, 192103.
(46) Lu Low, K.; Yang, Y.; Han, G.; Fan, W.; Yeo, Y. Electronic Band Structure and Effective Mass Parameters of Ge1−xSnx Alloys. *J. Appl. Phys.* **2012**, *112*, 103715.
(47) Stange, D.; von den Driesch, N.; Rainko, D.; Schulte-Braucks, C.; Wirths, S.; Mussler, G.; Tiedemann, A. T.; Stoica, T.; Hartmann, J. M.; Ikonic, Z.; Mantl, S.; Grützmacher, D.; Buca, D. Study of GeSn Based Heterostructures: Towards Optimized Group IV MQW LEDs. *Opt. Express* **2016**, *24*, 1358.
(48) Rainko, D.; Ikonic, Z.; Vukmirović, N.; Stange, D.; von den Driesch, N.; Grützmacher, D.; Buca, D. Investigation of Carrier Confinement in Direct Bandgap GeSn/SiGeSn 2D and 0D Heterostructures. *Sci. Rep.* **2018**, *8*, 1−13.

https://doi.org/10.1021/acsaelm.3c00112
ACS Appl. Electron. Mater. 2023, 5, 2268−2275